Article:
Zhao, J., Shi, D., Kaeufer, K. et al. (11 more authors) (Accepted: 2025) Strigolactones optimise plant water usage by modulating vessel formation. Nature Communications. ISSN 2041-1723 (In Press)

Strigolactones optimise plant water usage by modulating vessel formation

Jiao Zhao[1,*], Dongbo Shi[1,2,3,*,✉], Kiara Kaeufer[1,*], Changzheng Song[1], Dominik Both[1], Anna Lea Thier[1], Hui Cao[2], Linus Lassen[2], Xiaocai Xu[4], Yuki Hamamura[5], Laura Luzzietti[1], Tom Bennett[6], Kerstin Kaufmann[4], Thomas Greb[1,✉]

Affiliations:

[1]Developmental Physiology, Centre for Organismal Studies, Heidelberg University, Heidelberg, Germany

[2]Genetics, Institute of Biochemistry and Biology, University of Potsdam, Potsdam, Germany

[3]RIKEN Center for Sustainable Resource Science, Yokohama, Japan

[4]Plant Cell and Molecular Biology, Institute of Biology, Humboldt-Universität zu Berlin, Berlin, Germany

[5]Max Planck Institute of Molecular Plant Physiology, Potsdam, Germany

[6]School of Biology, Faculty of Biological Sciences, University of Leeds, Leeds, UK

✉correspondence: tohaku.seki@riken.jp, thomas.greb@cos.uni-heidelberg.de

*These authors contributed equally to this work.

Abstract

Wood formation is crucial for plant growth, enabling water and nutrient transport through vessel elements, derived from cambium stem cells (CSCs). CSCs produce vascular cell types in a bidirectional manner, but their regulation and cell fate trajectories remain unclear. Here, using single-cell transcriptome analysis in *Arabidopsis thaliana*, we reveal that the strigolactone (SL) signaling pathway negatively regulates vessel element formation, impacting plant water usage. While SL signaling is generally active in differentiating vascular tissues, it is low in developing vessels and CSCs, where it modulates cell fate decisions and drought response. SL-dependent changes in vessel element formation directly affect transpiration rates via stomata, underscoring the importance of vascular tissue composition in water balance. Our findings demonstrate the role of structural alignment in water-transport tissues under unstable water conditions, offering insights for enhancing drought resistance in plants through long-term modulation of vascular development.

Introduction

Continuous growth and tissue formation is one characteristic of plant development and important for aligning distinct body structures with changing environmental conditions. Cambium-driven radial growth of shoots and roots of dicotyledonous species is an important feature of this growth mode, and key for biomass production and for the long-term sequestration of CO_2[1]. CSCs proliferate usually providing wood (i.e. xylem) cells inwards and bast (i.e. phloem) cells outwards. Within xylem and phloem tissues, various cell types fulfil highly specialised functions like water transport by xylem vessel elements or sugar transport by phloem sieve elements[2]. However, mechanisms regulating CSC-associated cell fate decisions to cope with stressful environmental conditions are largely unknown.

Driven by transpiration at leaves and the resulting negative pressure in vessel elements, xylem-associated water transport is crucial for delivering water and dissolved minerals from the roots to the leaves, where photosynthesis occurs. Thus, disruptions in water transport, such as drought or embolism, can severely impair plant performance, reducing photosynthetic efficiency and metabolic rates, ultimately boosting drought-induced mortality [3]. The efficiency of water transport is a central parameter to ensure constant water supply under fluctuating water availability and, to a large extent, depends on the morphology and size of vessel elements. In fact, functions describing transpiration-based water loss indicate that the xylem is limiting for water transport when water is readily available[4]. Therefore, pathways actively modulating vessel element formation in response to alternating water availability are expected but have not been identified in the context of cambium-driven xylem formation.

Here, we provide cell-resolved transcriptomes of CSCs and all CSC-derived cell types generated by single nucleus RNA-sequencing (snRNA-seq). Based on our droplet- and plate-

based high-resolution transcriptome analysis, we identify SL signalling as a modulator of vessel formation and, thereby, as a module mediating structural adaptations to fluctuating water availability and drought stress.

Results

snRNA-seq analysis of radial growth

To comprehensively reveal cell states during radial plant growth, we established an snRNA-seq-based atlas of the Arabidopsis hypocotyl, the organ connecting shoot and root systems and being a hotspot for cambium-based organ growth[5]. To this end, nuclei were extracted, filtered, and purified via a cell sorter and processed by droplet-based single nucleus transcriptome analysis[6] (Fig. 1a, Supplementary Fig. 1a). Demonstrating the success of our approach, at least 400 transcribed genes were detected in 4,722 out of 6,780 processed nuclei. From those, we kept 2,061 high quality nuclei in which at least 1,200 unique molecular identifier (UMI) counts were identified for further analysis. Within these high quality nuclei, we detected 26,613 genes as being transcribed, covering nearly 70 % of the annotated genes for Arabidopsis[7]. On the median level, our analysis detected 1,224 transcribed genes and 1,854 UMIs for each nucleus (Supplementary Data 1).

By unsupervised clustering of the high-quality nuclei, we obtained 18 clusters, as visualised in a 'uniform manifold approximation and projection' (UMAP, Fig. 1b, Supplementary Data 2). Based on publicly available cell type-specific marker genes[8,9], we annotated cluster identities representing all major cell types reported for the hypocotyl (Fig. 1c, d, Supplementary Data 3). These cell types included the cambium (see below) and the periderm, which is a secondary protective tissue characterised by *MYB84*, *GLYCEROL-3-PHOSPHATE SN-2-ACYLTRANSFERASE5* (*GPAT5*), and *WUSCHEL RELATED HOMEOBOX4* (*WOX4*) expression[10]. As an exception, phloem sieve elements were not detected, presumably due to the absence of nuclei in those cells. Annotations were verified by promoter reporter analyses of selected genes marking vascular clusters (Supplementary Fig. 2). Importantly, we identified a CSC-associated cluster containing 139 nuclei specifically

expressing 151 genes including the known CSC markers *WOX4*[11–13], *PHLOEM INTERCALATED WITH XYLEM* (*PXY*)[11,14,15], *SUPPRESSOR OF MAX2 1-LIKE5* (*SMXL5*)[11,16], *AINTEGUMENTA* (*ANT*)[17,18], and *ARABIDOPSIS THALIANA HOMEOBOX8* (*ATHB8*)[19] (p-value adjusted based on Bonferroni correction (p_adj) < 0.01, Fig. 1d, Supplementary Data 2)[20]. Pseudotime analyses reconstructing developmental trajectories of vascular clusters revealed that vascular-related trajectories were linked to the CSC cluster (Fig. 1b). This was in remarkable contrast to previous analyses of procambium cells, the precursors of cambium cells during apical growth, which usually localise at the end of developmental trajectories[9]. Our trajectory analyses moreover allowed a more detailed clusterization along the differentiation path resulting in several clusters specifically representing small sections of the path (Supplementary Fig. 3, Supplementary Data 2). Collectively, our results revealed that CSCs hold a specific transcriptome and reflected the central role of CSCs as the developmental origin of cells driving radial plant growth.

To increase the analytic depth of our CSC characterization, we next applied the plate-based 'vast transcriptome analysis of single cells by dA-tailing' (VASA-seq) method[21] capturing both polyadenylated RNA and non-polyadenylated RNA, and used fluorescence intensity of the cambium domain reporters PXY_{pro}*:H4-GFP* and $SMXL5_{pro}$*:H2B-RFP*[11] during fluorescence-activated sorting to isolate 1,134 cambium nuclei (Supplementary Fig. 1b, c). In addition, we isolated the same number of nuclei from the whole hypocotyl without PXY_{pro}*:H4-GFP/*$SMXL5_{pro}$*:H2B-RFP*-based sorting. In total, we processed 2,268 nuclei resulting in 1,559 high quality nuclei showing at least 1,200 unique fragment identifier (UFI) counts/nucleus (Supplementary Fig. 4a, Supplementary Data 1). Overall, we detected transcripts of 33,195 genes including the two reporter transgenes, covering more than 85 % of the annotated genes in Arabidopsis. On the median level, our VASA-seq approach detected 2,688 genes/nucleus

and 5,210 UFI/nucleus, which matched previous high quality datasets for Arabidopsis nuclei[22].

Unsupervised clustering of the VASA-seq processed nuclei resulted in 19 clusters which we associated with distinct cell states using marker genes identified previously and during our droplet-based approach (Supplementary Fig. 4b, c). Again, most hypocotyl cell types were represented by a cluster in the VASA-seq dataset with a lower relative size of 'periderm' or 'developing vessel' clusters than obtained by our droplet-based approach presumably due to the depletion of those nuclei during the cambium-centred nucleus selection (Supplementary Data 2). Moreover, CSC marker genes were expressed this time in two clusters representing CSCs ('VASA_CSC' cluster, 94 nuclei) and dividing CSCs ('VASA_dividing' cluster, 66 nuclei) (Supplementary Fig. 4c) based on transcript abundance of genes previously associated with dividing root cells[9]. Supporting the conclusion that these were CSC nuclei, both clusters showed high GFP (*PXY_{pro}:H4-GFP*) and RFP (*$SMXL5_{pro}$:H2B-RFP*) fluorescence intensities[11] (Supplementary Fig. 5a). We furthermore identified 226 and 405 marker genes for each CSC cluster, respectively ($p\_adj < 0.01$, Supplementary Data 2) demonstrating that the VASA-seq analysis substantially increased analytical depth. Moreover, 119 of 151 (72 %) CSC marker genes identified by our droplet-based approach were included in the groups of CSC and/or dividing CSC marker genes (Supplementary Fig. 5b) and could be confirmed by expression analyses in plants (Supplementary Fig. 6), suggesting that results from both approaches were robust.

SL signalling activity within radial growth

Demonstrating their relevance, our cell-resolved transcriptome data recapitulated xylem-associated auxin signalling and phloem-associated cytokinin signalling[23] when we monitored transcript abundance of respective hormone-responsive genes[24] within identified

clusters (Supplementary Fig. 7). Interestingly, when we mapped the activity of 94 genes induced by the synthetic SL analogue GR24^{4DO} [25], we found that the expression of these genes was particularly low in the cluster representing dividing CSCs and in a subset of the xylem cell clusters, presumably representing differentiating vessel elements ('VASA_XPa', Fig. 2a, b). Indeed, when analysing SL signalling levels by the genetically encoded SL signalling sensor Strigo-D2[26], we found that SL-signalling activity was lower in CSCs and in developing vessel elements compared to phloem and xylem parenchyma cells (Fig. 2c–e). To find further support for this conclusions and to map the activity of SL-dependent genes in radially growing organs, we expressed an SL-resistant version of the proteolytic target of the SL-signalling pathway SMXL7 (SMXL7^{d53})[27] fused to the dexamethasone (DEX)-inducible GLUCOCORTICOID RECEPTOR (GR) under the control of the endogenous *SMXL7* promoter (*SMXL7$_{pro}$:SMXL7^{d53}-GR*). When performing transcriptional profiling of hypocotyls five hours after DEX application, we identified 1,022 DEX-induced and 409 DEX-suppressed genes (Supplementary Data 4) significantly overlapping with previously-reported GR24^{4DO}-suppressed and GR24^{4DO}-induced genes[25], respectively (Fig. 2f). This suggested that our analysis successfully identified genes downstream of SL signalling in the Arabidopsis hypocotyl. In line with results obtained using the Strigo-D2 sensor, in both VASA and 10x snRNA-seq datasets, DEX-suppressed genes showed significantly lower expression in clusters representing developing vessels and cambium stem cells when compared to xylem parenchyma and phloem clusters (Fig. 2g, h, Supplementary Fig. 8). Taken together, these results indicated that SL signalling levels are relatively low in developing vessels and in CSCs.

SLs are a class of carotenoid-derived phytohormones, modulating various processes including shoot branching and drought resistance[28,29]. SL molecules are perceived by the α/β hydrolase DWARF14 (D14) inducing interaction with the F-box protein MORE AXILLARY

GROWTH2 (MAX2) and thereby promoting degradation of the transcriptional regulators SMXL6, SMXL7, and SMXL8[25,30,31]. Using fluorescent promoter reporters, we found that the genes encoding these signalling components were widely active in the hypocotyl with a particular focus on the xylem (Supplementary Fig. 9): The activity of the *MAX2* reporter was detected in developing xylem vessels, xylem parenchyma cells, cambium cells and phloem parenchyma cells, whereas *D14* reporter activity was only detected in xylem parenchyma cells and phloem parenchyma cells. *SMXL6*, *SMXL7*, and *SMXL8* reporter activities were all detected in xylem parenchyma cells, with *SMXL7* also being detected in developing vessels (Supplementary Fig. 9). The transcripts of several SL biosynthetic genes were also widely detected both in xylem parenchyma cells and developing vessels (Supplementary Fig. 10). Our analyses thus associated SL signalling components with differentiating and differentiated vascular tissues and were in line with a regulatory role of the pathway in their formation.

SL-signalling suppresses vessel formation

To reveal a possible function of the SL-signalling pathway in vascular tissue formation, we next compared hypocotyls from *d14* mutants and wild type by again applying droplet-based snRNA-seq. After clustering and cluster annotation based on our initially identified genes marking the different hypocotyl cell types (Supplementary Fig. 11**,** Supplementary Data 1), we found that cell composition and transcriptional states were highly similar between the two genotypes (Fig. 3a). Interestingly, as the most prominent difference, we detected a three-fold increase in the abundance of nuclei from developing vessel elements (WTd14_devV) in *d14* mutants (Fig. 3b, Supplementary Fig. 11). Those were identified based on the expression of the *VASCULAR-RELATED NAC-DOMAIN6* (*VND6*), *VND7*[32,33] and *IRREGULAR XYLEM3* (*IRX3)*[34] and other xylem marker genes (Fig. 3c, Supplementary Fig. 11d–i). In line with an increased number of vessel elements, transcripts of *VND6*, *VND7* and

194 *IRX3* were more abundant in *d14* mutants (Fig. 3d). Indeed, histological analyses revealed a
195 higher density and increased size of vessel elements in both the SL signalling mutants *d14* and
196 *max2* (Fig. 3e–i) and the SL biosynthesis mutant *max1* (Supplementary Fig. 12a–c). This
197 alteration was not observed in *BRANCHED1* (*BRC1*)-defective plants (Supplementary Fig.
198 12d–f) which, similarly as *d14*, *max1*, and *max2* mutants, show increased branching[35], arguing
199 against the possibility that increased shoot formation causes enhanced vessel formation as a
200 secondary effect. Moreover, *KAI2*-deficient plants impaired in KARRIKIN signaling which,
201 like SL signaling, involves the F-box protein MAX2[36], did not show enhanced vessel formation
202 (Supplementary Fig. 12g–i), demonstrating that altered vessel formation specifically depends
203 on altered SL signaling.
204
205 In contrast to the SL signalling and biosynthesis mutants, the number and size of vessel
206 elements was decreased in *smxl6;smxl7;smxl8* (*smxl6;7;8*), *d14*;*smxl6;7;8* (Fig. 3e-i) and
207 *max2;smxl6;7;8* mutants (Supplementary Fig. 12j, k) demonstrating that increased vessel
208 formation in SL-related mutants depends on the proteolytic targets of the SL signalling
209 pathway. To this effect, mostly *SMXL7* and *SMXL8* contributed in a redundant fashion, as no
210 other *max2;smxl* double or triple mutant combination than *max2;smxl7;8* showed a mild
211 reduction in vessel density in comparison to *max2* (Supplementary Fig. 12j, k). Further
212 supporting a positive role of the proteolytic targets of SL-signalling in vessel formation,
213 expressing SMXL7^{d53}, the SL-resistant version of SMXL7[27], under the control of the *SMXL7*
214 promoter (*SMXL7$_{pro}$:SMXL7^{d53}-mVenus*) was sufficient to promote cambium-associated vessel
215 formation (Fig. 4a, b, e, f). Moreover, SMXL7^{d53}-GR-inducible genes were significantly
216 upregulated and SMXL7^{d53}-GR-repressible genes were significantly downregulated in *d14*
217 mutants in several vascular-related clusters (Fig. 3j), indicating that SL signalling indeed
218 regulates gene expression in vascular cells. In accordance with previous reports that SL

signalling negatively regulates the expression of auxin-dependent genes[25], we also found that auxin-inducible genes were significantly enriched in the group of SMXL7^{d53}-GR-inducible genes together with abscisic acid (ABA) and methyl jasmonate (MJ)-inducible genes (Fig. 3k). This result suggested a systematic negative effect of SL signalling on auxin, ABA and jasmonate signalling. With three SMXL7^{d53}-GR-inducible and 13 SMXL7^{d53}-GR-repressible genes specifically expressed in xylem parenchyma (VASA_XPb cluster) including the auxin transporter genes *PIN-FORMED 3* and *LIKE AUXIN RESISTANT 2* (Supplementary Data 3), we also identified candidates regulating the ratio of vessels and xylem parenchyma downstream of SL signalling. Along these lines, when reducing the activity of the HD ZIP-III transcription factor family, an established group of auxin-dependent xylem regulators, by inducing *miRNA165a* expression targeting all five *HD ZIP-III* mRNAs[17,37], the difference in vessel formation observed between wild type and the *SMXL7$_{pro}$:SMXL7^{d53}-mVenus* line, disappeared (Fig. 4 g–j). This argued for an essential role of the HD ZIP-III transcription factors downstream of the SL signaling pathway and for an influence of SL signaling on canonical regulators of xylem development.

Furthermore indicating a vascular-associated role of SL signalling, *d14* mutants did not show an increased vessel phenotype when they carried a transgene expressing *D14* under the control of the cambium- and early xylem-specific *WOX4* promoter (*WOX4$_{pro}$:D14*) (Fig. 4a, c–f). The same transgene had no effect in *max2* or *max1* mutants, demonstrating that the effect of *D14* depended on endogenous SL signalling and biosynthesis (Fig. 4k–q). Together with the observation that application of GR24^{4DO} specifically decreased vessel formation in wild type and *max1* but not in *d14* (Supplementary Fig. 13), we concluded that SL-signalling negatively regulates vessel formation during radial plant growth in cambium-derived cells and in an *SMXL6;7;8*-dependent fashion.

Vessel development influences transpiration

Relative water content is reduced in *d14* and *max2* mutants[38–40] and increased in *smxl6,7,8* triple mutants when grown in water-deprived pots[41], suggesting that SL signalling optimises water usage. Confirming this role, water usage was increased in *d14* and *max2* mutants and reduced in *smxl6;7;8* mutants (Supplementary Fig. 14a). ABA-induced closure of stomata, the main transpiration site in plants, is slower in SL signalling deficient mutants and proposed as one cause for their reduced drought resistance[38–40]. Indeed, stomatal conductance was elevated in *d14* and *max2* mutants and lower in *smxl6;7;8* mutants compared to wild type plants under both well-watered and water deficiency conditions (Supplementary Fig. 14b), demonstrating that transpiration is reduced by SL signalling. In contrast, *brc1* mutants showed a stomatal conductance like wild type again demonstrating that enhanced branching does not cause higher transpiration (Supplementary Fig. 14c). Moreover, we found a similar reduction of stomatal conductance in *d14;smxl6;7;8* and *max2;smxl6;7;8* mutants compared to *smxl6;7;8* mutants (Supplementary Fig. 14c) indicating that D14 and MAX2 require their downstream targets SMXL6, SMXL7 and SMXL8 for affecting transpiration. Again indicating that this effect depended on SL signalling in vascular tissues, *d14* mutants carrying a $WOX4_{pro}$*:D14* transgene showed normal transpiration rates and no altered stomata density (Supplementary Fig. 15a, b). In accordance with previous reports[39,40], stomata density was not changed in *d14* and *max2* mutants and only slightly enhanced in *smxl6;7;8* mutants (Supplementary Fig. 15b, c, d, e). Moreover, cuticle thickness was comparable between wild type and *d14* (Supplementary Fig. 15f) arguing against altered stomata density or cuticle defects as reasons for altered transpiration in SL-related mutants.

Further supporting an impact of vessel development on water usage, induction of a DEX-

inducible and auxin-insensitive version of the AUXIN RESPONSE FACTOR (ARF) transcription factor MONOPTEROS (MP, also known as ARF5) expressed under the control of the cambium-associated *PXY* promoter (*PXY$_{pro}$:GR-MPΔIII/IV*[11,42,43] resulted in a significant increase of vessel formation (Fig. 5a, b) and, at the same time, in elevated stomatal conductance in both well-watered and water deficiency condition (Fig. 5d). This effect was observed although stomata density was not significantly affected upon induction (Supplementary Fig. 15g, h). Interestingly, in wild type activation of auxin signalling by inducing MPΔIII/IV increased vessel number but reduced their size, while in *smxl6;7;8* mutants only the vessel number increased (Fig. 5a–c). This observation indicated that, in contrast to a common but independent effect of SL and auxin signalling on vessel number, both pathways have an interconnected effect on vessel size. Based on these findings, we rationalised that SL signalling restricts water usage in plants by modulating vessel formation and, consequently, water transport capacity. Supporting this idea, application of carboxyfluorescein diacetate (CFDA) to roots, used to study long distance transport along the xylem[44], resulted in higher fluorescence intensity in hypocotyls of *d14* mutants than in wild type (Fig. 5e, f).

To further explore the effect of reduced water availability on vessel formation and the role of SL-signalling in this process, we subjected wild type and *d14* plants for two weeks to a soil-based water deficiency treatment. As a result, smaller vessels with a thicker cell wall were formed in wild type, while only very few of those were formed in *d14* mutants (Fig. 5g, h). Likewise, when we reduced water availability for plants by adding 9 % polyethylene glycol (PEG_{8000}) to hydroponic cultures[45], fewer vessel elements with thickened cell walls were generated in *d14* than in wild type (Supplementary Fig. 14d, e). These observations showed that SL signalling promotes structural changes in vessel elements when plants experience water deficiency.

294

Discussion

Taken together, by starting off with a cell-resolved transcriptome analysis of radially growing Arabidopsis organs, we revealed that SL signalling modifies the number and size of vessel elements produced during cambium-dependent radial growth. The possibility to modulate vessel anatomy in response to environmental cues like drought[46], can be assumed to be an important fitness trait and has, so far, been described for being mediated by ABA signalling during longitudinal growth[47]. We did, however, neither observe any alteration of primary vessel element formation in primary *d14* roots (Supplementary Fig. 16a), nor an increase of cambium-derived vessel formation in *aba deficient 2* (*aba2*) mutants (Supplementary Fig. 16d, f) impaired in ABA biosynthesis[48] and showing higher stomatal conductance[49]. Moreover, the formation of cambium-derived vessel elements was not altered in mutants displaying an increased stomatal density and a resulting increase in stomatal conductance[50,51] (Supplementary Fig. 16e, f), arguing against a positive effect of enhanced transpiration on vessel formation. These findings suggest that ABA- and SL-signalling pathways fulfil distinct functions with regard to their effect on vessel formation during primary and secondary development, respectively. Based on the observation that increased vessel formation by enhancing auxin signaling also leads to enhanced transpiration, there is indeed the possibility that increased stomatal conductance in SL-related mutants is a result of enhanced vessel element formation and an associated increase of water transport along the vascular system.

Interestingly, SL biosynthesis is enhanced in rice roots in drought conditions[52] indicating that the pathway has the potential to lead to structural changes when plants experience growth, to possibly anticipate harsh conditions in the future. Depending on distinct ecological or agricultural niches plants have adapted to, it may be advantageous to establish a

320 weaker or stronger impact of SL signalling on vessel element formation to cope with distinct
321 environmental regimes.

Methods

Plant material

All plant lines used in this study were *Arabidopsis thaliana* (L.) Heynh. plants of the accession Columbia (Col-0). The single and higher order mutants of *d14-1* (WiscDsLoxHs137_07E), *smxl6-4* (SALK_049115), *smxl7-3* (WiDsLox339_C04), *smxl8-1* (SALK_025338C), *max1-1*, and *max2-1* were obtained from Dave Nelson[53,54] (UC Riverside, US) and Ottoline Leyser[55] (SLCU, Cambridge, UK). The *35S$_{pro}$:XVE>>miRNA165a* line was received from Ari Pekka Mähönen[17] (University of Helsinki, Finland). The *brc1-2* (SALK_091920) mutant was ordered from NASC and was characterised previously[35,56–58]. *Strigo-D2*[26], *PXY$_{pro}$:ER-ECFP-HDEL*[59], *PXY$_{pro}$:H4-GFP;SMXL5$_{pro}$:H2B-RFP*[11], *SMXL7$_{pro}$:SMXL7^{d53}-VENUS*[27], *PXY$_{pro}$:Myc-GR-bdl*[42], *MP$_{pro}$:ER-EYFP-HDEL*[42], and *PXY$_{pro}$:GR-MPΔIII/IV*[42] transgenic lines were described previously. Other transgenic lines were generated through the floral dipping method using *Agrobacterium tumefaciens*[60]. The *aba2-11* mutant[48] was obtained from Mikael Brosché (University of Helsinki, Finland). *epf1-1* (SALK_137549)[61] and *epf2-3* (SALK_047918)[62] single and double mutants and *tmm-1* (SALK_011958)[63] mutants were kindly donated by Christopher Grefen (University of Bochum, Germany). *PFA1$_{pro}$:PFA1-GFP*[64] lines were obtained from Tatsuo Kakimoto (Osaka University, Japan).

Vector construction

The *WOX4$_{pro}$:D14* (*pVJ13*) construct was generated using In-Fusion cloning (Takara Bio) using the amplified *D14* coding region and BamHI-digested *pTOM49*[13]. Other plasmids were generated using the GreenGate cloning system[65,66]. *SMXL7^{d53}* in pGGC (*pJZ60*) was mutagenised based on the template of the *SMXL7* CDS in pGGC (*pKR07*) according to the manual of the QuickChange Site-Directed Mutagenesis Kit (Agilent, Santa Clara, USA). See

Supplementary Data 5 for oligo sequences used for molecular cloning and Supplementary Data 6 for each module used during the cloning process.

Growth conditions

Arabidopsis seeds were surface sterilised by 70 % ethanol containing 0.02 % Tween-20, stratified at 4°C for 2-3 days in the dark, sown on 0.8 % w/v agar in 1/2 Murashige and Skoog (MS) medium supplemented with 1 % w/v sucrose. Seedlings were grown in short-day conditions (SD; 10 h light and 14 h darkness) at 21-22°C. For morphological observations and reporter activity analyses, five day-old seedlings were transferred to pots filled with 4:1 mixture of soil and vermiculite. After 21 days, plants were transferred to long day conditions (LD; 16 h light and 8 h darkness) at 21-22°C. Plants for stomatal conductance measurements were grown for six weeks in SD conditions (8.5 h light and 15.5 h darkness).

Single nucleus RNA-seq analysis

Hypocotyls were dissected and collected in petri dishes incubated on ice. 2 ml of 1x nuclei isolation buffer (CelLytic™ PN Isolation/Extraction Kit, Sigma #CELLYTPN1) supplemented with 20 µl RiboLock RNase inhibitor 40 U/µL (ThermoFisher #EO0381) and Hoechst 33342 at 10 µg/ml final concentration were prepared and a minimum amount of buffer was applied to submerge the collected hypocotyls[10]. Hypocotyls were chopped using razor blades (Wilkinson Sword) for up to 5 min and then gently shaken at 4°C for 15 min. Samples were then filtered through a 50 µm filter (CellTrics, Sysmex #04-004-2327) and passed to a low protein binding tube (Eppendorf #0030108132).

For 10x genomics application, 50,000 nuclei were sorted into 33 µl collection buffer (10 µl PBS (Corning, #21-040-CV), 5 µl BSA (ThermoFisher, #AM2616), 6 µl RNAse inhibitor (ThermoFisher, #AM2682), 12 µl RNAse inhibitor (ThermoFisher, #AM2694)), modified from a previous report[67], by a BD FACSAria IIIu cell sorter (Becton Dickinson) using a 100-µm sort nozzle (see Supplementary Fig. 1). A sheath pressure of 35 psi and a drop drive frequency of 60 kHz were applied. 43.2 µl of sorted nuclei solution was applied to a Chromium Next GEM Chip without dilution and Chromium Next GEM Single Cell 3' GEM, Library & Gel Bead Kit (v3.1) was used to generate libraries following the manufacturer's instruction. Nuclei concentration was monitored by a fluorescent cell counter (ThermoFisher, Countess 3 FL) using the DAPI channel to obtain approximately 200 nuclei/µl. Libraries were sequenced using a NextSeq (Illumina) machine at the high output mode.

For initial wild type analyses, about 100 hypocotyls from a *PXY_{pro}:H4-GFP;$SMXL5_{pro}$:H2B-RFP* line collected four weeks after germination were used. Sequencing reads were mapped to the Arabidopsis genome (with H4GFP and H2BRFP transgene sequences added) using STAR (2.7.8a)[68] with the "--alignIntronMax 10000 --alignMatesGapMax 10000" option. "GeneFull" option was used in STAR solo to include reads mapped to introns. Seurat[69] (4.0.6, 4.1.0 or 4.3.0) was used for further analysis. Cells with nCount_RNA between 1201 and 9999 and a mitochondrial genome read fraction of less than 20 % were kept for further analysis. Clustering and UMAP were generated using default settings of Seurat with the parameters "dims = 1:15, resolution =1.2, algorithm =2". Monocle 3 (1.3.1)[70].

For wild type and *d14* mutant analysis, about 200 hypocotyls collected 19 days after germination were used. Sequencing reads were mapped to the Arabidopsis nuclear genome with cell ranger (6.0.1, 10x genomics) using the "--include-introns" and "--alignIntronMax 10000 --alignMatesGapMax 10000" alignment options. nCount_RNA between 1501 and

14999 were kept for comparing wild type and *d14* mutants. Clustering was carried out using parameters „dims = 1:15, resolution =1.2, algorithm =2“, and UMAPs were generated after randomly resampling 500 nuclei from each genotype.

For VASA-seq analysis[21], about 100 hypocotyls from a *PXY$_{pro}$:H4-GFP;SMXL5$_{pro}$:H2B-RFP* line were collected four weeks after germination to obtain 1,134 ‘cambium region’ nuclei (three 384-well plates). Additional 100 hypocotyls were used for collecting 1,134 ‘all region’ nuclei (three 384-well plates) (see Supplementary Fig. 1). Single nuclei were sorted into individual wells of 384-well plates containing well index oligos purchased from Single Cell Discoveries B.V. (Utrecht, The Netherlands), using the index sorting mode of the BD FACSAria IIIu cell sorter, recording the fluorescence signal of each nucleus (Supplementary Data 7). Multi-well plates were frozen and further processed according to the VASA-seq protocol[21] of Single Cell Discoveries with the following modifications. 1) In the end repair and polyA reactions, our added mix per well contained 7.5 µM ATP and 3.75 mU of polyA polymerase. 2). We used 6 µl of ExoSAP after *in vitro* transcription. 3) The composition of our 2,5x RNaseH buffer used during the rRNA depletion step was 125 mM Tris-HCl pH 7.5, 250 mM NaCl, 10 mM $MgCl_2$. Sequencing reads were similarly mapped to the Arabidopsis genome (with H4GFP and H2BRFP transgene sequences added) using STAR with the same options mentioned above. Well barcodes were obtained from Gene Expression Omnibus (https://www.ncbi.nlm.nih.gov/geo/; Accession ID: GSE112438, celseq2_bc.csv.gz). Fluorescent signals were combined in Seurat with a 150 offset value to avoid negative values in the 488 nm and 561 nm channels and all nucleus data were merged. Cells with nCount_RNA values between 1201 and 14999, a mitochondrial genome read fraction lower than 20 %, fluorescent signals in the 405 nm and 488 nm channels lower than 75,000 were kept for further analysis. Clustering and UMAP were performed with parameters „dims = 1:15, resolution =1.8, algorithm =2“.

Basic statistics of all single cell analyses can be found in Supplementary Data 1. Marker genes for each cluster were generated by using the *FindAllMarkers* function in Seurat (Supplementary Data 2) (only.pos = TRUE, min.pct = 0.25, logfc.threshold = 0.25, test ="wilcox", return.thresh = 0.01). Seurat object files for each dataset are deposited at Gene Expression Omnibus under accession code GSE224928 [https://www.ncbi.nlm.nih.gov/geo/query/acc.cgi?acc=GSE224928]. Phytohormone responsive genes[24,25] and marker genes for cell clusters generated by single cell transcriptome analyses[8,9,71] were curated from previous reports and integrated in Seurat by using the AddModuleScore function (Supplementary Data 3). Differential expression was tested by the Steel-Dwass test using an R script (http://aoki2.si.gunma-u.ac.jp/R/src/Steel-Dwass.R) authored by Shigenobu Aoki (Gunma University, Japan).

Confocal Microscopy

Hypocotyl samples were fixed overnight at 4°C in 4 % (w/v) PFA dissolved in PBS. The tissue was washed twice with PBS, optionally embedded in 5 % low gelling temperature agarose, sectioned by razor blades (Wilkinson basic), and then stained with 0.1 % DirectRed 23, 0.1 % Renaissance SR2200 (Renaissance Chemicals Ltd, UK) or 10 µg/ml Hoechst 33342 for 5 min at room temperature. Excess staining was removed by clearing the sample in 1X PBS. Confocal microscopy experiments were carried out on a Leica TCS SP8 (Leica Microsystems Mannheim, Germany). 458 nm, 514 nm and 561 nm lasers were used to excite mTurquoise2 (CFP), YFP (mVenus), and mCherry/Direct Red, and emissions were detected at 465-509 nm, and 524-540 nm and 571-630 nm, respectively. Hoechst 33342 and Calcofluor White, together with lignin in differentiated xylem vessel elements were visualised using a 405 nm laser, and collection of the emission at 410-450 nm. Basic Fuchsin was visualised using a 561 nm laser

by STELLARIS 8 (Leica Microsystems, Mannheim, Germany) or Leica TCS SP8 (Leica Microsystems Mannheim, Germany), collecting the emission in a range of 586-650 nm. Imaging of promoter reporter lines for cluster annotation validation and *in situ* hybridization were carried out on an LSM 710 (Carl Zeiss Microscopy GmbH, Oberkochen, Germany) or on a STELLARIS 8 (Leica Microsystems, Mannheim, Germany). 405 nm, 488 nm, 561 nm lasers were used to excite Renaissance SR2200, GFP, Direct Red 23 and ATTO550, respectively.

Hybridization chain reaction (HCR)-based *in situ* hybridization

Arabidopsis hypocotyls from four week-old plants were fixed overnight at 4°C in 4 % (w/v) PFA. After washing off the fixative, sections were produced manually and immediately transferred to 100 % methanol for more than 5 min. Hybridization and amplification were carried out with ISHpalette Short hairpin amplifier ATTO550-S41 (#IPL-R-S41, Nepa Gene Co., Ltd., Ichikawa, Japan) according to the manufacturer's instructions. See Supplementary Data 5 for oligo sequences used as probes for each gene.

Strigo-D2 ratio analysis

False colour images were generated using ImageJ through calculating intensity ratios of each pixel from mVenus and mCherry channels after being Gaussian Blurred and subtracting background signals. For calculating the ratio value of each nucleus, nuclear regions were detected by using the Particle Analyzer function in ImageJ after masking the nuclear region through thresholding. Then, nuclear mVenus and mCherry signal intensity were measured and intensity ratios were determined. Nuclei within cambium, phloem, and xylem zones, as well as in developing vessel elements were manually defined as follow: around six cell layers counting from the vessel element border toward the organ periphery were defined as cambium zone.

Nuclei distal to the cambium were defined as phloem and the nuclei proximal to the cambium were defined as xylem. The enlarged nuclei within the xylem region were considered as being located in developing vessel elements.

Histological analyses

The harvested hypocotyls from five week-old (3 weeks SD + 2 weeks LD) plants or four week-old plants subjected to two weeks of water deficiency treatment (SD conditions) were infiltrated by 70 % ethanol for at least three days at 4°C before being paraffin embedded by the Leica ASP200 S processor (Leica Microsystems, Mannheim, Germany). After embedding in paraffin, the microtome RM2235 (Leica Microsystems, Mannheim, Germany) was used to produce 10-µm thick sections. The sections were harvested from the upper part of the hypocotyl, 1 mm below the leaf primordia. Dried sections were deparaffinized, stained with 0.05 % toluidine blue (#52040, AppliChem, Darmstadt, Germany) and fixed by Micromount Mounting Media (Leica Microsystems; Mannheim, Germany) on microscope slides (Thermo Scientific; Wal-tham, USA). Slides were scanned using the Pannoramic SCAN II scanner (3DHistech, Budapest, Hungary) and analysed by the CaseViewer 2.2 software (3DHistech, Budapest, Hungary). Vessel elements were either automatically detected using a developed vessel-counting macro in Fiji or the VesselWizard tool both established for this purpose[72] and corrected manually to eliminate false positives or negatives (using the Wand Tool in Fiji).

Dexamethasone and estradiol treatment

For *SMXL7*$_{pro}$*:SMXL7*^{d53}*-GR* induction by DEX, a stock solution of 25 mM DEX was dissolved in DMSO, and a 15 µM working solution was freshly prepared by diluting the stock solution with tap water. Control treatments contained an equivalent amount of solvent. Plants were

initially grown in SD conditions for three weeks without treatment, and treatment was started when plants were transferred to LD conditions by watering twice a week with either 50 ml 15 µM DEX or mock solution per pot until harvest. For estradiol induction of *35S:XVE>>miRNA165a* expression[17], a 20 mM stock solution of 17β-Estradiol (Sigma-Aldrich, E2758) was prepared in DMSO and stored at −20 °C. Five-day-old seedlings were transferred to plates supplemented with either 5 µM 17β-Estradiol or an equal volume of DMSO until they reached two weeks of age. Hypocotyls were harvested and fixed in 4 % PFA at 4 °C. Cross-sections, 200 µm thick, were obtained using a Vibratome (Leica VT1000 S) after embedding the samples in low-melting agarose (Sigma-Aldrich, A9414). The sections were stained overnight at 4°C with 0.02% Basic Fuchsin in ClearSee.

GR24^{4DO} application

2 µM GR24^{4DO} (StrigoLab S.r.l., c/o Dept. of Chemistry, Turin University, Italy) was prepared through a 5000x dilution of a stock solution (10 mM GR24^{4DO} dissolved in acetone). Seedlings were initially grown on plates containing solid 1/2 MS medium with 1 % sucrose supplemented for five days (SD conditions) without treatment, subsequently transferred to culture vessels (C1958, PhytoTechLabs, USA) supplemented either with 2 µM GR24^{4DO} or mock solution containing an equivalent amount of acetone, grown in SD condition and harvested four weeks after germination for histological analyses.

RNAseq and qRT-PCR analysis

1) RNAseq

DEX (Sigma-Aldrich, USA) was dissolved in DMSO as a 25 mM stock solution and stored at -20 °C. The working concentration of DEX was 15 µM diluted from the stock solution by tap water. The DEX-based induction of *SMXL7*$_{pro}$*:SMXL7*^{d53}*-GR* lines was conducted by directly watering 15 µM DEX or an equal volume of DMSO (mock) to four week-old plants (three weeks SD conditions then transferred to LD conditions) grown on soil. After five hours of incubation, the hypocotyls from DEX- and mock-treated plants were immediately harvested and ground using pestle and mortar after being immersed in liquid nitrogen. RNA was isolated using the RNeasy Mini Kit (QIAGEN, Netherland) and genomic DNA contamination was removed by referring to the protocol of TURBO DNA-free™ Kit (Thermo Scientific; USA). Subsequent clean-up of RNA was performed by using RNeasy Mini Kit. 1.2 µg of total RNA/sample was used for library preparation using NEBNext Ultra II RNA Library Prep Kit for Illumina (NEB) using the polyA mRNA workflow and Unique Dual Index primers (NEB). 12 cycles of amplification were performed and the libraries were sequenced using NextSeq 550 (Illumina). Obtained reads were mapped by STAR-2.7.8a with "--alignIntronMax 10000 --alignMatesGapMax 10000 --outFilterMultimapNmax 1" option. Reads per gene were counted by summarizeOverLaps function (GenomicAlignments v1.30.0)[73] with "mode="union", ignore.strand = TRUE" option. Differentially expressed genes were detected using DESeq2 (v1.34.0)[74] applying a threshold of “baseMean>50, |log2FoldChange|>0.585, padj<0.01”. Functional enrichment analysis was performed using g:GOSt (version: e111_eg58_p18_f463989d)[75].

2) qRT-PCR

Hypocotyls of four week-old wild type and *d14* mutant plants grown on soil were harvested. Total RNA was extracted using the method mentioned above. cDNA synthesis was performed

536 according to the instructions of the Thermo Revert Aid Kit (Thermo Scientific; Wal-tham,
537 USA). Real-time PCR assays were conducted using SYBR Green Mix (Thermo Scientific;
538 Wal-tham, USA) and gene-specific primers (Supplementary Data 5) on a qTOWER3 thermal
539 cycler and using the *EF1-a* (*AT5G60390*) gene as an internal reference.

540

541 **Water deficiency treatments**

542 To grow plants under comparable conditions, each pot contained 70 g of soil. For watering,
543 pots were placed in petri dishes to soak 25 ml water overnight from below. Next, 20 ml of
544 nematode-containing solution was added to each pot from above. For pot weight measurement,
545 pots were kept in petri dishes during subsequent watering (20 ml every week during the first
546 three weeks and 25 ml twice a week for the last two weeks). Pot weight was measured starting
547 five weeks after germination for the consecutive 12 days. For histological analysis of stress
548 related phenotypes, plants were grown well watered for two weeks (20 ml every week), before
549 water deficiency treatment was applied for two weeks. The control group was kept in well
550 watered conditions during the treatment.

551

552 **Stomatal conductance measurements**

553 Wild type, *d14*, *max2* and *smxl6;7;8* plants were grown in growth chambers with sufficient
554 watering for four weeks, followed by water deficiency treatments for 12 days. During the first
555 three weeks, plants were watered with 20 ml every week during the first three weeks and 30
556 ml twice a week for the next three weeks. DEX or mock-treated *PXY$_{pro}$:GR-MPΔIII/IV* plants
557 were not watered for 10 days after the DEX or DMSO treatment. Stomatal conductance of wild
558 type, *d14*, *max2* and *smxl6;7;8* plants was measured after 12 days of water deficiency treatment
559 and DEX or mock-treated *PXY$_{pro}$:GR-MPΔIII/IV* plants were analysed after 10 days of water

deficiency treatments. For the measurements, the SC-1 Leaf Porometer (METER Environment®, Meter Group, Pullman, US) was clipped on the abaxial side of the leaf. The 9th, 10th and 11th produced leaf of wild type, *smxl6;7;8,* DEX or mock-treated *PXY$_{pro}$:GR-MPΔIII/IV* plants and three well expanded upper leaves from *d14* or *max2* mutants were chosen for the measurement. The SC-1 Leaf Porometer was used according to the user manual. Single measurements were temporarily randomised across the course of the day and across genotypes.

Stomata imprints

Water deficiency-treated plants used for the stomatal conductance measurement were taken to imprint the abaxial leaf side for stomata density quantification (stomata/mm^2). For the imprint, a small drop of instant adhesive glue (UHU Sekundenkleber blitzschnell; UHU, Bühl, Germany) was placed on a Superfrost™ Microscope slide and the leaf was gently pressed on the glue for two seconds. The imprints were visualised using a Contrast Microscope DMIRB microscope with a 20x objective and the bright field mode. Five images of the central leaf regions of each imprint were taken. The number of stomata was counted using Fiji.

CFDA application

Roots of three week-old plants (grown on plates) were cut 2 cm below the hypocotyl and 5 µl of 1 mM CFDA (5(6)-Carboxyfluorescein diacetate N-succinimidyl ester, Sigma-Aldrich, USA) or DMSO were applied. After 30 min, hypocotyls were harvested, fixed with 4 % PFA and embedded in 9 % low gelling temperature agarose. 100 µm thick vibratome sections were used for confocal microscopy.

583 **Basic Fuchsin staining**

584 To observe xylem strands in roots, five day-old seedlings were stained and fixed in 0.2 % (m/v)
585 Basic Fuchsin dissolved in ClearSee[76,77] (10 % xylitol, 15 % sodium deoxycholate, and 25 %
586 UREA) solution overnight. Next the fuchsin solution was removed and samples were washed
587 once with ClearSee for 30 min. Subsequently, seedlings were stored in ClearSee solution and
588 analysed.

589

590 **Statistics & Reproducibility**

591 All the measurements were done on distinct samples. Statistical tests were applied in a two-
592 sided mode. Box plots indicate the 25th (Q1, box limit), 50th (median, centre line) and 75th
593 (Q3, box limit) percentiles and whiskers indicate the value range or up to the 1.5x interquartile
594 range from the Q1 or Q3 limit, respectively. Data points beyond this range were plotted
595 individually as outliers. Statistical analyses were carried out using R (v4.0.4 or v4.0.5), ggplot2
596 (v3.3.3), or Python (v3.10.7), pandas (v1.5.0), rstatix (v0.7.2) and seaborne (v0.12.0).

597 No statistical methods were used for sample-size calculation. Sample sizes have been
598 maximized according to practical considerations. No data were excluded from the analyses
599 except in snRNA-seq analysis, nuclei with a low number of molecules detected were excluded
600 from further analysis according to the standard pre-established analysis pipeline. All the
601 findings were confirmed by usually three but and at least two replicates. snRNA-seq analyses
602 were not replicated using the exactly same method and type of samples, however, findings
603 were confirmed in each analysis using different technologies and type of samples suggesting
604 their universality. Plant pot positions were randomized in possible cases, however,
605 randomization was not applied to all the experiments due to practical reasons (enhanced
606 physical handling of plants). Covariates were controlled by applying the exact same conditions

607 (growth substrate, temperature, light) to all individuals. The investigators were not blinded to
608 allocation during experiments and outcome assessment.

Data availability

Source data for each plot are provided with this paper. The raw sequencing data of snRNA-seq and bulk RNA-seq analyses, and Seurat object files of snRNA-seq data generated in this study have been deposited at NCBI's Gene Expression Omnibus database under accession code GSE224928 [https://www.ncbi.nlm.nih.gov/geo/query/acc.cgi?acc=GSE224928] or GSE270808 [https://www.ncbi.nlm.nih.gov/geo/query/acc.cgi?acc=GSE270808]. The authors declare that all other data supporting the findings of this study are mentioned in the main text or the supplementary materials.

Code availability

General codes used for analyses and specific parameters are provided in the Method section. Codes for presented vessel identification tools are deposited at Github [https://github.com/thomasgreb/Zhao-et-al_SL-vessels][72].

References

1. Bar-On, Y. M., Phillips, R. & Milo, R. The biomass distribution on Earth. *Proc Natl Acad Sci USA* **115**, 6506–6511 (2018).
2. Evert, R. F. & Eichhorn, S. E. *Esau's Plant Anatomy: Meristems, Cells, and Tissues of the Plant Body: Their Structure, Function, and Development, 3rd Edition*. 624 (Wiley-Liss, 2006).
3. Brodersen, C. R., Roddy, A. B., Wason, J. W. & McElrone, A. J. Functional status of xylem through time. *Annu. Rev. Plant Biol.* **70**, 407–433 (2019).
4. Sperry, J. S. & Love, D. M. What plant hydraulics can tell us about responses to climate-change droughts. *New Phytol.* **207**, 14–27 (2015).
5. Chaffey, N., Cholewa, E., Regan, S. & Sundberg, B. Secondary xylem development in Arabidopsis: a model for wood formation. *Physiol. Plant.* **114**, 594–600 (2002).
6. Zheng, G. X. Y. *et al.* Massively parallel digital transcriptional profiling of single cells. *Nat. Commun.* **8**, 14049 (2017).
7. Cheng, C.-Y. *et al.* Araport11: a complete reannotation of the *Arabidopsis thaliana* reference genome. *Plant J.* **89**, 789–804 (2017).
8. Tenorio Berrío, R. *et al.* Single-cell transcriptomics sheds light on the identity and metabolism of developing leaf cells. *Plant Physiol.* **188**, 898–918 (2022).
9. Wendrich, J. R. *et al.* Vascular transcription factors guide plant epidermal responses to limiting phosphate conditions. *Science* **370**, (2020).
10. Wunderling, A. *et al.* A molecular framework to study periderm formation in Arabidopsis. *New Phytol.* **219**, 216–229 (2018).
11. Shi, D., Lebovka, I., López-Salmerón, V., Sanchez, P. & Greb, T. Bifacial cambium stem cells generate xylem and phloem during radial plant growth. *Development* **146**,

(2019).

12. Hirakawa, Y., Kondo, Y. & Fukuda, H. TDIF peptide signaling regulates vascular stem cell proliferation via the WOX4 homeobox gene in Arabidopsis. *Plant Cell* **22**, 2618–2629 (2010).
13. Suer, S., Agusti, J., Sanchez, P., Schwarz, M. & Greb, T. WOX4 imparts auxin responsiveness to cambium cells in Arabidopsis. *Plant Cell* **23**, 3247–3259 (2011).
14. Fisher, K. & Turner, S. PXY, a receptor-like kinase essential for maintaining polarity during plant vascular-tissue development. *Curr. Biol.* **17**, 1061–1066 (2007).
15. Hirakawa, Y. *et al.* Non-cell-autonomous control of vascular stem cell fate by a CLE peptide/receptor system. *Proc Natl Acad Sci USA* **105**, 15208–15213 (2008).
16. Agusti, J., Lichtenberger, R., Schwarz, M., Nehlin, L. & Greb, T. Characterization of transcriptome remodeling during cambium formation identifies *MOL1* and *RUL1* as opposing regulators of secondary growth. *PLoS Genet.* **7**, e1001312 (2011).
17. Smetana, O. *et al.* High levels of auxin signalling define the stem-cell organizer of the vascular cambium. *Nature* **565**, 485–489 (2019).
18. Randall, R. S. *et al.* AINTEGUMENTA and the D-type cyclin CYCD3;1 regulate root secondary growth and respond to cytokinins. *Biol. Open* **4**, 1229–1236 (2015).
19. Baima, S. *et al.* The expression of the Athb-8 homeobox gene is restricted to provascular cells in Arabidopsis thaliana. *Development* **121**, 4171–4182 (1995).
20. Satija, R., Farrell, J. A., Gennert, D., Schier, A. F. & Regev, A. Spatial reconstruction of single-cell gene expression data. *Nat. Biotechnol.* **33**, 495–502 (2015).
21. Salmen, F. *et al.* High-throughput total RNA sequencing in single cells using VASA-seq. *Nat. Biotechnol.* **40**, 1780–1793 (2022).
22. Sunaga-Franze, D. Y. *et al.* Single-nucleus RNA sequencing of plant tissues using a nanowell-based system. *Plant J.* **108**, 859–869 (2021).

23. Immanen, J. *et al.* Cytokinin and auxin display distinct but interconnected distribution and signaling profiles to stimulate cambial activity. *Curr. Biol.* **26**, 1990–1997 (2016).
24. Nemhauser, J. L., Hong, F. & Chory, J. Different plant hormones regulate similar processes through largely nonoverlapping transcriptional responses. *Cell* **126**, 467–475 (2006).
25. Wang, L. *et al.* Transcriptional regulation of strigolactone signalling in Arabidopsis. *Nature* **583**, 277–281 (2020).
26. Song, C. *et al.* Strigo-D2-a bio-sensor for monitoring spatio-temporal strigolactone signaling patterns in intact plants. *Plant Physiol.* **188**, 97–110 (2022).
27. Liang, Y., Ward, S., Li, P., Bennett, T. & Leyser, O. SMAX1-LIKE7 Signals from the Nucleus to Regulate Shoot Development in Arabidopsis via Partially EAR Motif-Independent Mechanisms. *Plant Cell* **28**, 1581–1601 (2016).
28. Ranjan, A., Sinha, R., Singla-Pareek, S. L., Pareek, A. & Singh, A. K. Shaping the root system architecture in plants for adaptation to drought stress. *Physiol. Plant.* **174**, e13651 (2022).
29. Waters, M. T., Gutjahr, C., Bennett, T. & Nelson, D. C. Strigolactone signaling and evolution. *Annu. Rev. Plant Biol.* **68**, 291–322 (2017).
30. Yao, R. *et al.* DWARF14 is a non-canonical hormone receptor for strigolactone. *Nature* **536**, 469–473 (2016).
31. Shabek, N. *et al.* Structural plasticity of D3-D14 ubiquitin ligase in strigolactone signalling. *Nature* **563**, 652–656 (2018).
32. Kubo, M. *et al.* Transcription switches for protoxylem and metaxylem vessel formation. *Genes Dev.* **19**, 1855–1860 (2005).
33. Yamaguchi, M. *et al.* VASCULAR-RELATED NAC-DOMAIN7 directly regulates the expression of a broad range of genes for xylem vessel formation. *Plant J.* **66**, 579–590

(2011).

34. Taylor, N. G., Scheible, W. R., Cutler, S., Somerville, C. R. & Turner, S. R. The irregular xylem3 locus of Arabidopsis encodes a cellulose synthase required for secondary cell wall synthesis. *Plant Cell* **11**, 769–780 (1999).
35. Aguilar-Martínez, J. A., Poza-Carrión, C. & Cubas, P. Arabidopsis *BRANCHED1* acts as an integrator of branching signals within axillary buds. *Plant Cell* **19**, 458–472 (2007).
36. Nelson, D. C. *et al.* F-box protein MAX2 has dual roles in karrikin and strigolactone signaling in Arabidopsis thaliana. *Proc Natl Acad Sci USA* **108**, 8897–8902 (2011).
37. Zhong, R. & Ye, Z.-H. Regulation of HD-ZIP III Genes by MicroRNA 165. *Plant Signal. Behav.* **2**, 351–353 (2007).
38. Ha, C. V. *et al.* Positive regulatory role of strigolactone in plant responses to drought and salt stress. *Proc Natl Acad Sci USA* **111**, 851–856 (2014).
39. Bu, Q. *et al.* Regulation of drought tolerance by the F-box protein MAX2 in Arabidopsis. *Plant Physiol.* **164**, 424–439 (2014).
40. Li, W. *et al.* Comparative functional analyses of DWARF14 and KARRIKIN INSENSITIVE 2 in drought adaptation of Arabidopsis thaliana. *Plant J.* **103**, 111–127 (2020).
41. Li, W. *et al.* Negative Roles of Strigolactone-Related SMXL6, 7 and 8 Proteins in Drought Resistance in Arabidopsis. *Biomolecules* **10**, (2020).
42. Brackmann, K. *et al.* Spatial specificity of auxin responses coordinates wood formation. *Nat. Commun.* **9**, 875 (2018).
43. Krogan, N. T., Ckurshumova, W., Marcos, D., Caragea, A. E. & Berleth, T. Deletion of MP/ARF5 domains III and IV reveals a requirement for Aux/IAA regulation in Arabidopsis leaf vascular patterning. *New Phytol.* **194**, 391–401 (2012).

44. Melnyk, C. W., Schuster, C., Leyser, O. & Meyerowitz, E. M. A Developmental Framework for Graft Formation and Vascular Reconnection in Arabidopsis thaliana. *Curr. Biol.* **25**, 1306–1318 (2015).
45. He, Q. *et al.* Endogenous Salicylic Acid Levels and Signaling Positively Regulate Arabidopsis Response to Polyethylene Glycol-Simulated Drought Stress. *J. Plant Growth Regul.* **33**, 871–880 (2014).
46. Awad, H., Barigah, T., Badel, E., Cochard, H. & Herbette, S. Poplar vulnerability to xylem cavitation acclimates to drier soil conditions. *Physiol. Plant.* **139**, 280–288 (2010).
47. Ramachandran, P., Wang, G., Augstein, F., de Vries, J. & Carlsbecker, A. Continuous root xylem formation and vascular acclimation to water deficit involves endodermal ABA signalling via miR165. *Development* **145**, (2018).
48. González-Guzmán, M. *et al.* The short-chain alcohol dehydrogenase ABA2 catalyzes the conversion of xanthoxin to abscisic aldehyde. *Plant Cell* **14**, 1833–1846 (2002).
49. Kalliola, M. *et al.* Differential role of MAX2 and strigolactones in pathogen, ozone, and stomatal responses. *Plant Direct* **4**, e00206 (2020).
50. Hepworth, C., Doheny-Adams, T., Hunt, L., Cameron, D. D. & Gray, J. E. Manipulating stomatal density enhances drought tolerance without deleterious effect on nutrient uptake. *New Phytol.* **208**, 336–341 (2015).
51. Papanatsiou, M., Amtmann, A. & Blatt, M. R. Stomatal spacing safeguards stomatal dynamics by facilitating guard cell ion transport independent of the epidermal solute reservoir. *Plant Physiol.* **172**, 254–263 (2016).
52. Haider, I. *et al.* The interaction of strigolactones with abscisic acid during the drought response in rice. *J. Exp. Bot.* **69**, 2403–2414 (2018).
53. Soundappan, I. *et al.* SMAX1-LIKE/D53 Family Members Enable Distinct MAX2-

749 Dependent Responses to Strigolactones and Karrikins in Arabidopsis. *Plant Cell* **27**,
750 3143–3159 (2015).
751 54. Stanga, J. P., Smith, S. M., Briggs, W. R. & Nelson, D. C. SUPPRESSOR OF MORE
752 AXILLARY GROWTH2 1 controls seed germination and seedling development in
753 Arabidopsis. *Plant Physiol.* **163**, 318–330 (2013).
754 55. Stirnberg, P., Furner, I. J. & Ottoline Leyser, H. M. MAX2 participates in an SCF
755 complex which acts locally at the node to suppress shoot branching. *Plant J.* **50**, 80–94
756 (2007).
757 56. Niwa, M. *et al.* BRANCHED1 interacts with FLOWERING LOCUS T to repress the
758 floral transition of the axillary meristems in Arabidopsis. *Plant Cell* **25**, 1228–1242
759 (2013).
760 57. Alonso, J. M. *et al.* Genome-wide insertional mutagenesis of *Arabidopsis thaliana*.
761 *Science* **301**, 653–657 (2003).
762 58. Finlayson, S. A. Arabidopsis Teosinte Branched1-like 1 regulates axillary bud
763 outgrowth and is homologous to monocot Teosinte Branched1. *Plant Cell Physiol.* **48**,
764 667–677 (2007).
765 59. Agusti, J. *et al.* Strigolactone signaling is required for auxin-dependent stimulation of
766 secondary growth in plants. *Proc Natl Acad Sci USA* **108**, 20242–20247 (2011).
767 60. Clough, S. J. & Bent, A. F. Floral dip: a simplified method for *Agrobacterium*-mediated
768 transformation of *Arabidopsis thaliana*. *Plant J.* **16**, 735–743 (1998).
769 61. Unable to find information for 384393.
770 62. Hara, K. *et al.* Epidermal cell density is autoregulated via a secretory peptide,
771 EPIDERMAL PATTERNING FACTOR 2 in Arabidopsis leaves. *Plant Cell Physiol.*
772 **50**, 1019–1031 (2009).
773 63. Sugano, S. S. *et al.* Stomagen positively regulates stomatal density in Arabidopsis.

Nature **463**, 241–244 (2010).

64. Zhang, Y. *et al.* Two types of bHLH transcription factor determine the competence of the pericycle for lateral root initiation. *Nat. Plants* **7**, 633–643 (2021).
65. Lampropoulos, A. *et al.* GreenGate---a novel, versatile, and efficient cloning system for plant transgenesis. *PLoS ONE* **8**, e83043 (2013).
66. Schürholz, A.-K. *et al.* A comprehensive toolkit for inducible, cell type-specific gene expression in Arabidopsis. *Plant Physiol.* **178**, 40–53 (2018).
67. Neumann, M. *et al.* A 3D gene expression atlas of the floral meristem based on spatial reconstruction of single nucleus RNA sequencing data. *Nat. Commun.* **13**, 2838 (2022).
68. Dobin, A. *et al.* STAR: ultrafast universal RNA-seq aligner. *Bioinformatics* **29**, 15–21 (2013).
69. Hao, Y. *et al.* Integrated analysis of multimodal single-cell data. *Cell* **184**, 3573-3587. (2021).
70. Trapnell, C. *et al.* The dynamics and regulators of cell fate decisions are revealed by pseudotemporal ordering of single cells. *Nat. Biotechnol.* **32**, 381–386 (2014).
71. Shahan, R. *et al.* A single-cell Arabidopsis root atlas reveals developmental trajectories in wild-type and cell identity mutants. *Dev. Cell* **57**, 543-560.e9 (2022).
72. Zhao, J. & Both, D. Vessel counting tools used for "Strigolactones optimise plant water usage by modulating vessel formation." *Zenodo* (2025) doi:10.5281/zenodo.15094693.
73. Lawrence, M. *et al.* Software for computing and annotating genomic ranges. *PLoS Comput. Biol.* **9**, e1003118 (2013).
74. Love, M. I., Huber, W. & Anders, S. Moderated estimation of fold change and dispersion for RNA-seq data with DESeq2. *Genome Biol.* **15**, 550 (2014).
75. Kolberg, L. *et al.* g:Profiler-interoperable web service for functional enrichment analysis and gene identifier mapping (2023 update). *Nucleic Acids Res.* **51**, W207–W212 (2023).

76. Ursache, R., Andersen, T. G., Marhavý, P. & Geldner, N. A protocol for combining fluorescent proteins with histological stains for diverse cell wall components. *Plant J.* **93**, 399–412 (2018).

77. Kurihara, D., Mizuta, Y., Sato, Y. & Higashiyama, T. ClearSee: a rapid optical clearing reagent for whole-plant fluorescence imaging. *Development* **142**, 4168–4179 (2015).

Acknowledgements

10x Chromium operation, library preparation and next-generation sequencing were carried out by David Ibberson (The CellNetworks Deep Sequencing Core Facility, Heidelberg University, Germany). For data storage, we used the SDS@hd service of Heidelberg University. Nucleus sorting was carried out by Monika Langlotz (Flow Cytometry and FACS Core Facility, ZMBH, Heidelberg University, Germany). VASA-seq processing was carried out by Single Cell Discoveries B.V. (Utrecht, The Netherlands). We thank David Nelson (University of California Riverside, USA), Christopher Grefen (University of Bochum, Germany), Mikael Brosché (University of Helsinki, Finland), Ottoline Leyser (University of Cambridge, UK) for providing plant material, Virginie Jouannet (Heidelberg University, Germany) for generating plant material, Arun Sampathkumar (Max Planck Institute of Molecular Plant Physiology, Germany) and Jan Lohmann (Heidelberg University, Germany) for sharing equipment. We also thank Tiago Daniel Gomes Nunes (Heidelberg University, Germany) and Michael Raissig (University of Bern, Switzerland) for support in stomatal conductance measurements. Moreover, we thank Kiyoshi Mashiguchi and Shinjiro Yamaguchi (Kyoto University, Kyoto, Japan) for technical support. This work was supported by a fellowship of the Chinese Scholarship Council (CSC) and a Peterson scholarship (http://www.peterson-elites.sdu.edu.cn/jxjjj.htm) to J.Z., an overseas research fellowship of the Japan Society for the Promotion of Science [JSPS Overseas 201960008] to D.S.. Ki.K. was supported by a doctoral fellowship of the Landesgraduiertenförderung of the state Baden-Württemberg. Y.H. was supported by the Max Planck Gesellschaft. Work in T.G.'s group was furthermore supported by the SFB 1101 of the Deutsche Forschungsgemeinschaft (DFG), the DFG project GR 2104/10-1 and the ERC consolidator grant PLANTSTEMS. Work in the D.S.'s group was supported by the JST PRESTO grant [JPMJPR2046] and the DFG projects 504847536 and 512328399. Work in the Ke.K. group was supported by the DFG projects 438774542 and 512328399.

Author contributions statement

J.Z., D.S., Ki.K. and T.G. designed the study. J.Z., D.S., H.C., Li.L., Ki.K., D.B., A.L.T., and La.L. performed experiments. J.Z., D.S., Ki.K. and C.S. analysed the data. X.X. and Ke.K. provided technical support on single nucleus RNA-seq analysis. Y.H. provided technical support on microscopy. T.B. provided essential material. J.Z., D.S. and T.G. wrote the manuscript with input from all the authors.

Competing interests statement

The authors declare no competing interests.

Additional information

Supplementary Information is available for this paper.

Correspondence and requests for material should be addressed to Dongbo Shi (tohaku.seki@riken.jp) or Thomas Greb (thomas.greb@cos.uni-heidelberg.de).

Figure legends

Fig. 1: Identification of Arabidopsis hypocotyl cell types using 10x Chromium snRNA-seq.

a, Sample collection pipeline. **b,** UMAP plot of 10x Chromium snRNA-seq analysis using 2,061 Arabidopsis hypocotyl nuclei organised in 18 clusters obtained through unsupervised clustering analysis. Differentiation trajectory based on pseudo-time analysis originating from CSCs is shown by black lines in the right-bottom. A scheme of major hypocotyl cell types is shown in the top left corner. **c**, **d**, Dot plot showing the expression of tissue-specific and stage-specific marker genes identified in previous scRNA-seq analyzes[8,9,71] (**c**) and previously characterised tissue-specific marker genes (**d**) in the identified clusters (y-axis, shared between **c** and **d**). The size of the circles represents the percentage of cells with expression (percent expressed), whereas the colour indicates the scaled average expression (average expression). XPa-dV: xylem parenchyma and developing vessels; XP: xylem parenchyma; CSC: cambium stem cells; devP: developing phloem; CC: companion cells; PP: phloem parenchyma; devC: developing cortex; cortex-EPI: cortex-epidermis. Source data are provided as a Source Data file.

Fig. 2: Strigolactone (SL) signalling in the radially expanding hypocotyl.

a, **b**, Violin plot (**a**) and UMAP visualisation (**b**) of expression profiles of 94 $GR24^{4DO}$-induced genes[25] in cambium-related cell clusters identified by VASA-seq. Statistical groups determined by the Steel-Dwass test for multiple comparisons are indicated by letters ($p < 0.05$). Gene lists used in this analysis can be found in Supplementary Data 3. A close-up of the UMAP originated from the VASA-seq cluster identification (Supplementary Fig. 4) is shown as a reference. **c,** Maximum intensity projection of confocal microscopy images of 5-week-old hypocotyl cross-sections expressing Strigo-D2 (*$35S_{pro}$:SMXL6-D2-mVenus_$35S_{pro}$:mCherry-NLS*) as an indicator of SL signalling. mVenus and mCherry signals are shown in green and magenta, respectively. Hoechst33342 was used to stain nuclei shown in blue together with the autofluorescence of lignified cell walls in vessel elements. Yellow arrowheads indicate the nuclei of developing vessel elements. Size bars represent 100 µm and 20 µm on the left and right, respectively. **d**, Ratiometric images of mVenus / mCherry signals after image processing (see Methods). The colour bar indicates the scale of ratio values from 0 to 6. Higher ratio indicates lower SL signalling levels. **e**, Box plot showing nuclear fluorescence intensity ratio of mVenus and mCherry in different vascular tissues. Data from one individual plant are shown in the same colour (n=5). The total number of nuclei analysed for each tissue type of five plants was 42 (developing vessels), 389 (xylem parenchyma), 903 (cambium), and 411 (phloem). Statistical groups are indicated by letters and assessed by a one-way ANOVA with post-hoc Tukey-HSD (95 % CI) on the mean ratio value of each tissue type in each individual plant. **f**, Venn diagram showing the overlap of *$SMXL7_{pro}$:$SMXL7^{d53}$-GR* DEX-induced genes and $GR24^{4DO}$-suppressed genes, and of *$SMXL7_{pro}$:$SMXL7^{d53}$-GR* DEX-suppressed genes and $GR24^{4DO}$-induced genes. Results of Fisher's exact test are shown. **g**, **h**, UMAP visualisation (**g**) and violin plot (**h**) of expression profiles of DEX-induced and DEX-suppressed genes in the cambium-related cell clusters identified by VASA-seq. Statistical groups determined by the Steel-Dwass test for multiple comparisons are indicated by letters ($p < 0.05$). Source data are provided as a Source Data file. For box plot definition, please see Methods-Statistics section.

Fig. 3: Effect of SL signalling on vessel development.

a, UMAP plot of 10x Chromium snRNA-seq analysis using 500 hypocotyl nuclei organised in 15 clusters obtained through unsupervised clustering. 500 nuclei were randomly resampled from 684 (WT) and 684 (*d14*) nuclei, respectively. Abbreviations for annotated clusters are devV: developing vessel; XP: xylem parenchyma; CSC/X: cambium stem cell/xylem; CSC/P: cambium stem cell/phloem; devP: developing phloem; CC: companion cell; PP: phloem parenchyma; devC: developing cortex; EPI: epidermis. **b**, Changes in relative nuclei abundance for each cluster in *d14* mutants compared to wild type. Fisher's exact test was used to determine statistical differences in each cluster between genotypes. * p<0.05, ** p<0.01. p = 1.0e-03 (cluster 1:WTd14_devP), p = 3.1e-03 (cluster 3:WTd14_periderm), p = 2.9e-07 (cluster 6:WTd14_devV). **c**, Expression of the developing vessel marker genes *VND6*, *VND7* and *IRX3* in the UMAP plot shown in a. **d**, Relative transcript abundance of *VND6*, *VND7* and *IRX3* in *d14* mutants compared to wild type, normalised to the *EF-1a* reference gene in qRT-PCR experiments. n = 3 biological replicates. **e**, Toluidine-blue stained hypocotyl cross-sections from five week-old wild type, *d14*, *max2*, *smxl6;7;8* and *d14;smxl6;7;8* plants. Vessels were automatically identified using ImageJ and subsequent manual correction (marked in red). Scale bar represents 50 µm. **f**–**i**, Quantification of the vessel element numbers per section (**f**), the average area of individual vessel elements (**g**), the total vessel area per section (**h**) and the ratio between the vessel element area and the total xylem area (**i**) in different genotypes. n=15 (WT), 15 (*d14*), 13 (*max2*), 10 (*smxl6;7;8*), 14 (*d14;smxl6;7;8*) plants for each genotype. Statistical groups are indicated by letters and determined by a one-way ANOVA with post-hoc Tukey-HSD (95 % CI). **j**, Violin plot of expression profiles of DEX-induced and DEX-suppressed genes (SMXL7^{d53}-GR) in the cambium-related cell clusters identified by the WT-d14 10x snRNA-seq dataset. Statistical groups for wild type expression patterns determined by the Steel-Dwass test for multiple comparisons are indicated by letters (p < 0.05). Asterisks indicate significant difference of transcript abundance between wild type and *d14* mutants in each cluster, respectively (Steel-Dwass test, p<0.05). p = 1.6e-03 (cluster 8, induced), 2.2e-02 (cluster 1, induced), 4.1e-02 (cluster 6, suppressed), 3.1e-02 (cluster 10, suppressed), 4.3e-07 (cluster 8, suppressed), 2.4e-03 (cluster 12, suppressed), 5.4e-07 (cluster 1, suppressed). p values are also shown in the Source Data file. **k**, Enrichment of DEX-induced (top) or DEX-suppressed (bottom) genes in phytohormone responsive gene lists curated from Nemhauser et al., 2006[24]. Bonferroni corrected p value of Fisher's one-tailed test is shown in a negative $\log_{10}$ format. IAA: indole 3 acetic acid (auxin); CK: zeatin (cytokinin); ABA: abscisic acid; ACC: 1-amino-cyclopropane-1-carboxylic acid (ethylene precursor); BL: brassinosteroid; MJ: methyl jasmonate (jasmonate); GA: gibberellic acid (gibberellin). Source data are provided as a Source Data file. For box plot definition, please see Methods-Statistics section.

Fig. 4: Analysis of *SMXL7$_{pro}$:SMXL7^{d53}-mVenus*, *WOX4$_{pro}$:D14/d14*, *WOX4$_{pro}$:D14/max2*, and *WOX4$_{pro}$:D14/max1* plants.

a–**d**, Toluidine blue-stained hypocotyl cross-sections from 5 week-old wild type (**a, b**) and *d14* (**c, d**) plants carrying a *SMXL7$_{pro}$:SMXL7^{d53}-mVenus* (**b**) or *WOX4$_{pro}$:D14* (**d**) transgene. Vessel elements were automatically identified using ImageJ and subsequent manual correction (marked in red). **e**, **f**, Quantification of vessel element number per section (**e**) and mean vessel element area size per section (**f**) comparing wild type, *d14*, three independent lines carrying *WOX4$_{pro}$:D14* transgenes in the *d14* background and lines carrying a *SMXL7$_{pro}$:SMXL7^{d53}-mVenus* transgene. n=11 (WT), 13 (*SMXL7$_{pro}$:SMXL7^{d53}-mVenus*/WT), 12 (*d14*) and 9 (*WOX4$_{pro}$:D14*/d14) plants for each genotype. This assay was conducted in parallel with the *brc1* vessel element analysis, and both share the same wild type data. **g, h,** Basic Fuchsin-

stained hypocotyl cross-sections from 2 week-old *35S$_{pro}$:XVE>>miRNA165a* transgenic plants in wild type (**g**) and *SMXL7$_{pro}$:SMXL7^{d53}-mVenus* background (**h**), following *miRNA165a* induction by 17β-Estradiol (17-β) in 5-day-old seedlings. **i**, **j**, Quantification of vessel element number per section (**i**) and mean vessel element area size per section (**j**). n = 17 (WT, Mock), 22 (WT, 17-β), 17 (*SMXL7$_{pro}$:SMXL7^{d53}-mVenus*, Mock) and 25 (*SMXL7$_{pro}$:SMXL7^{d53}-mVenus*, Mock, 17-β) plants for each group. **k-o**, Toluidine blue-stained hypocotyl cross-sections from five week-old wild type (**k**), *max2* (**l**), *max2* plants carrying a *WOX4$_{pro}$:D14* transgene (**m**), *max1* (**n**) and *max1* plants carrying a *WOX4$_{pro}$:D14* transgene (**o**). Vessel elements were automatically identified using ImageJ and subsequent manual correction (marked in red). **p**, **q**, Quantification of vessel element number per section (**p**) and mean vessel element area size per section (**q**). n=8 (WT), 11 (*max2*), 11 (*WOX4$_{pro}$:D14/max2*), 10 (*max1*) and 13 (*WOX4$_{pro}$:D14/max1*) plants for each genotype. Statistical groups are indicated by letters and were determined by a one-way ANOVA with post-hoc Tukey-HSD (95 % CI). Scale bar represents 50 µm. Source data are provided as a Source Data file. For box plot definition, please see Methods-Statistics section.

Fig. 5: Effect of altered vessel formation on water usage and stomatal conductance

a, Toluidine blue-stained hypocotyl cross-sections of five week-old plants carrying a *PXY$_{pro}$:GR-MPΔIII/IV* transgene in wild type or in *smxl6;7;8* triple mutants. Plants were treated with mock or DEX solutions for the last two weeks. Vessels were automatically identified using ImageJ and subsequent manual correction (marked in red). Scale bar represents 100 µm. **b**, **c**, Vessel element numbers per section (**b**) and individual vessel element area mean per section (**c**) in response to DEX treatment comparing wild type and *smxl6;7;8* mutants as shown in **a**. n=12 (WT, Mock), 16 (WT, DEX), 14 (*smxl6;7;8*, Mock), 16 (*smxl6;7;8*, DEX) plants for each group. Asterisks indicate $p<0.01$ in the post-hoc Bonferroni correction after one-way ANOVA for the effect of treatment for each genotype. p=6.8e-09 (WT, **b**), p=3.6e-05 (*smxl6;7;8*, **b**), p=2.9e-09 (WT, **c**), p=0.35 (*smxl6;7;8*, **c**). **d**, Quantification and comparison of stomatal conductance in *PXY$_{pro}$:GR-MPΔIII/IV* plants treated with mock or DEX solution under well-watered or water-deficiency (10 days) conditions. Stomatal conductance of three leaves was measured per plant using an SC1 Leave prometer. n=15 plants for each condition. The asterisk indicates significance when the two-sided Welch's t-test was applied, * $p < 0.01$, p=2.8e-03 (well-watered), p=4.9e-09 (10 days water deficiency). **e**, Hypocotyl cross sections of wild type and *d14* plants after CFDA staining. Xylem autofluorescence shown in blue and CFDA-derived signal in green. **f**, Quantification of CFDA signal intensity between WT and *d14* in hypocotyl cross sections shown in g. Scale bar indicates 50 µm. n=33 plants (wild type) and 23 plants (*d14*). p=6.5e-05 (two-sided Welch's t-test). **g**, Toluidine blue-stained hypocotyl vessel elements of five week-old plants subjected to a soil-based water deficiency treatment. Vessels were automatically identified using VesselWizard and subsequent manual correction. Stress-related vessels are marked with asterisks. Scale bar represents 100 µm. **h**, Quantification of stressed vessel element number between wild type and *d14*. The asterisk indicates significance when the two-sided Welch's t-test was applied, * $p < 0.01$, p=2.1e-06. n=21 plants (wild type) and 15 plants (*d14*). Source data are provided as a Source Data file. For box plot definition, please see Methods-Statistics section.

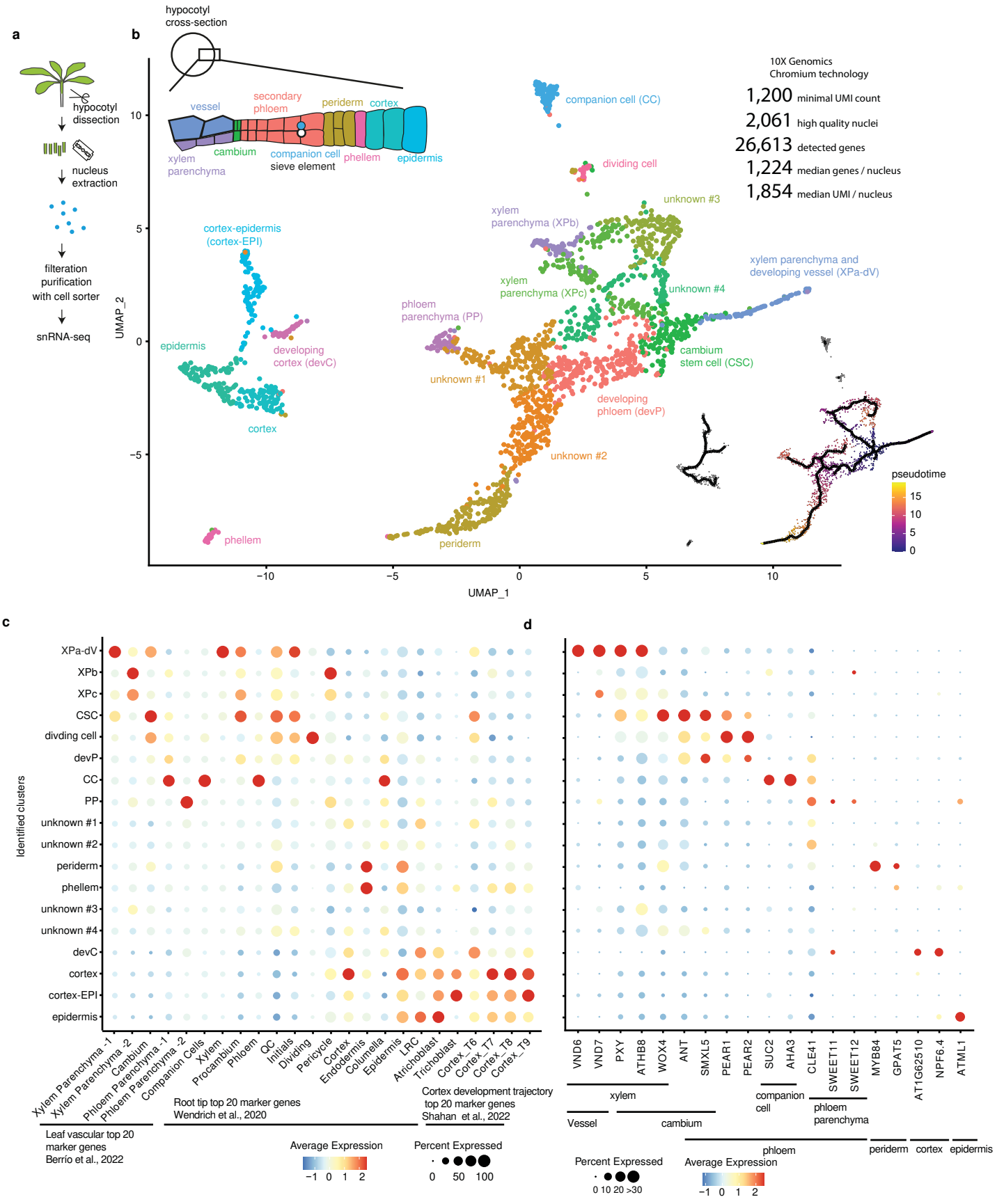
a
hypocotyl dissection
nucleus extraction
filteration purification with cell sorter
snRNA-seq
b
hypocotyl cross-section
vessel
secondary phloem
periderm
cortex
xylem parenchyma
cambium
companion cell
sieve element
phellem
epidermis
10X Genomics Chromium technology
1,200 minimal UMI count
2,061 high quality nuclei
26,613 detected genes
1,224 median genes / nucleus
1,854 median UMI / nucleus
companion cell (CC)
dividing cell
unknown #3
xylem parenchyma (XPb)
xylem parenchyma and developing vessel (XPa-dV)
cortex-epidermis (cortex-EPI)
xylem parenchyma (XPc)
unknown #4
phloem parenchyma (PP)
epidermis
developing cortex (devC)
cambium stem cell (CSC)
unknown #1
developing phloem (devP)
cortex
unknown #2
phellem
periderm
pseudotime
15
10
5
0
UMAP_2
UMAP_1
10
5
0
−5
−10
−5
0
5
10
c
Identified clusters
XPa-dV
XPb
XPc
CSC
divding cell
devP
CC
PP
unknown #1
unknown #2
periderm
phellem
unknown #3
unknown #4
devC
cortex
cortex-EPI
epidermis
Xylem Parenchyma -1
Xylem Parenchyma -2
Cambium
Phloem Parenchyma -1
Phloem Parenchyma -2
Companion Cells
Xylem
Procambium
Phloem
QC
Initials
Dividing
Pericycle
Cortex
Endodermis
Columella
Epidermis
LRC
Atrichoblast
Trichoblast
Cortex_T6
Cortex_T7
Cortex_T8
Cortex_T9
Leaf vascular top 20 marker genes Berrío et al., 2022
Root tip top 20 marker genes Wendrich et al., 2020
Cortex development trajectory top 20 marker genes Shahan et al., 2022
Average Expression
−1 0 1 2
Percent Expressed
0 50 100
d
VND6
VND7
PXY
ATHB8
WOX4
ANT
SMXL5
PEAR1
PEAR2
SUC2
AHA3
CLE41
SWEET11
SWEET12
MYB84
GPAT5
AT1G62510
NPF6.4
ATML1
xylem
Vessel
cambium
companion cell
phloem parenchyma
phloem
periderm
cortex
epidermis
Percent Expressed
0 10 20 >30
Average Expression
−1 0 1 2

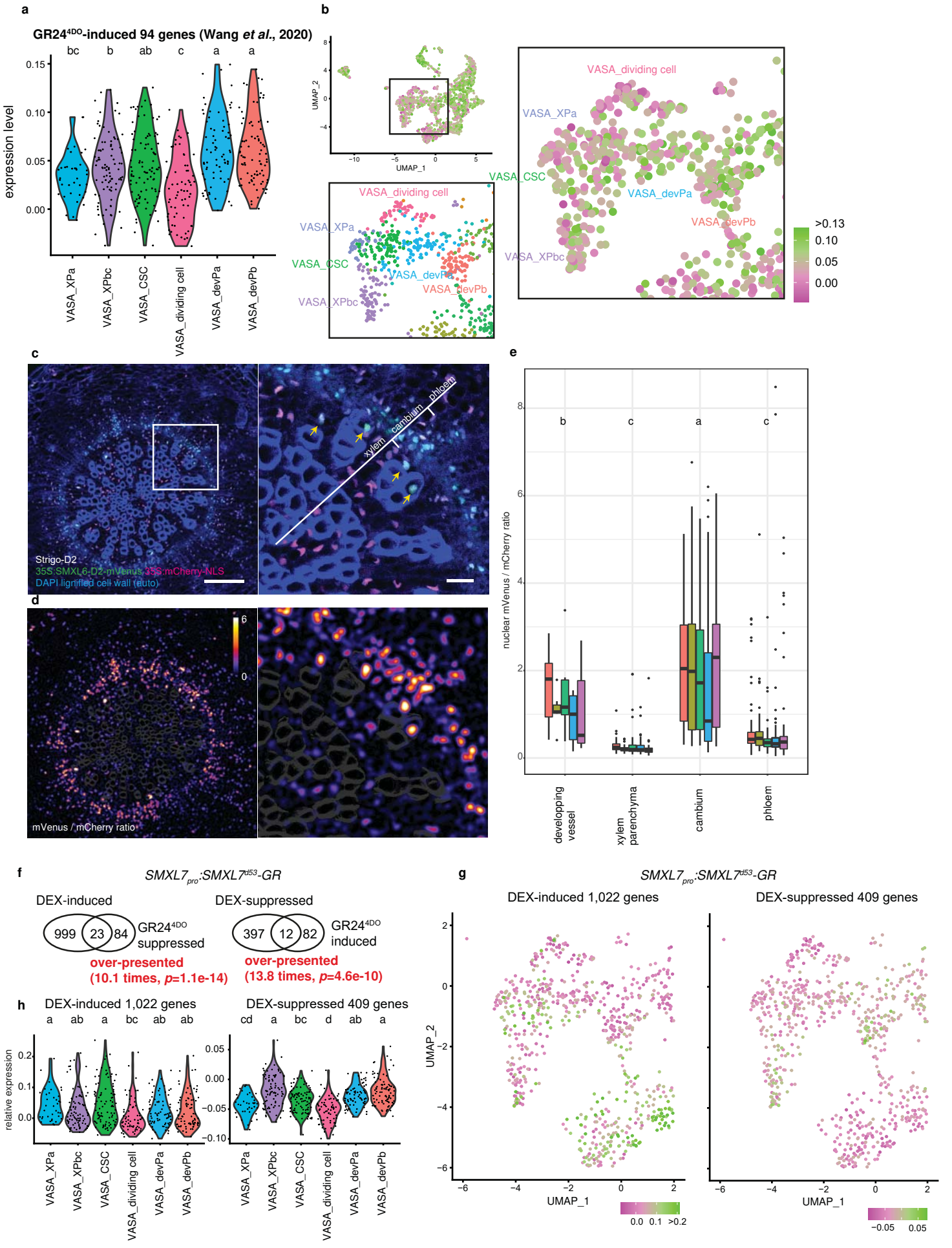
a
GR24^4DO-induced 94 genes (Wang et al., 2020)
bc b ab c a a
expression level
0.15
0.10
0.05
0.00
VASA_XPa
VASA_XPbc
VASA_CSC
VASA_dividing cell
VASA_devPa
VASA_devPb
b
UMAP_2
UMAP_1
VASA_dividing cell
VASA_XPa
VASA_CSC
VASA_devPa
VASA_devPb
VASA_XPbc
>0.13
0.10
0.05
0.00
c
Strigo-D2
35S:SMXL6-D2-mVenus 35S:mCherry-NLS
DAPI lignified cell wall (auto)
xylem
cambium
phloem
d
6
0
mVenus / mCherry ratio
e
nuclear mVenus / mCherry ratio
b c a c
developping vessel
xylem parenchyma
cambium
phloem
f
SMXL7pro:SMXL7d53-GR
DEX-induced
999 23 84
GR24^4DO suppressed
over-presented
(10.1 times, p=1.1e-14)
DEX-suppressed
397 12 82
GR24^4DO induced
over-presented
(13.8 times, p=4.6e-10)
g
SMXL7pro:SMXL7d53-GR
DEX-induced 1,022 genes
DEX-suppressed 409 genes
UMAP_2
UMAP_1
0.0 0.1 >0.2
−0.05 0.05
h
DEX-induced 1,022 genes
a ab a bc ab ab
DEX-suppressed 409 genes
cd a bc d ab a
relative expression
VASA_XPa
VASA_XPbc
VASA_CSC
VASA_dividing cell
VASA_devPa
VASA_devPb

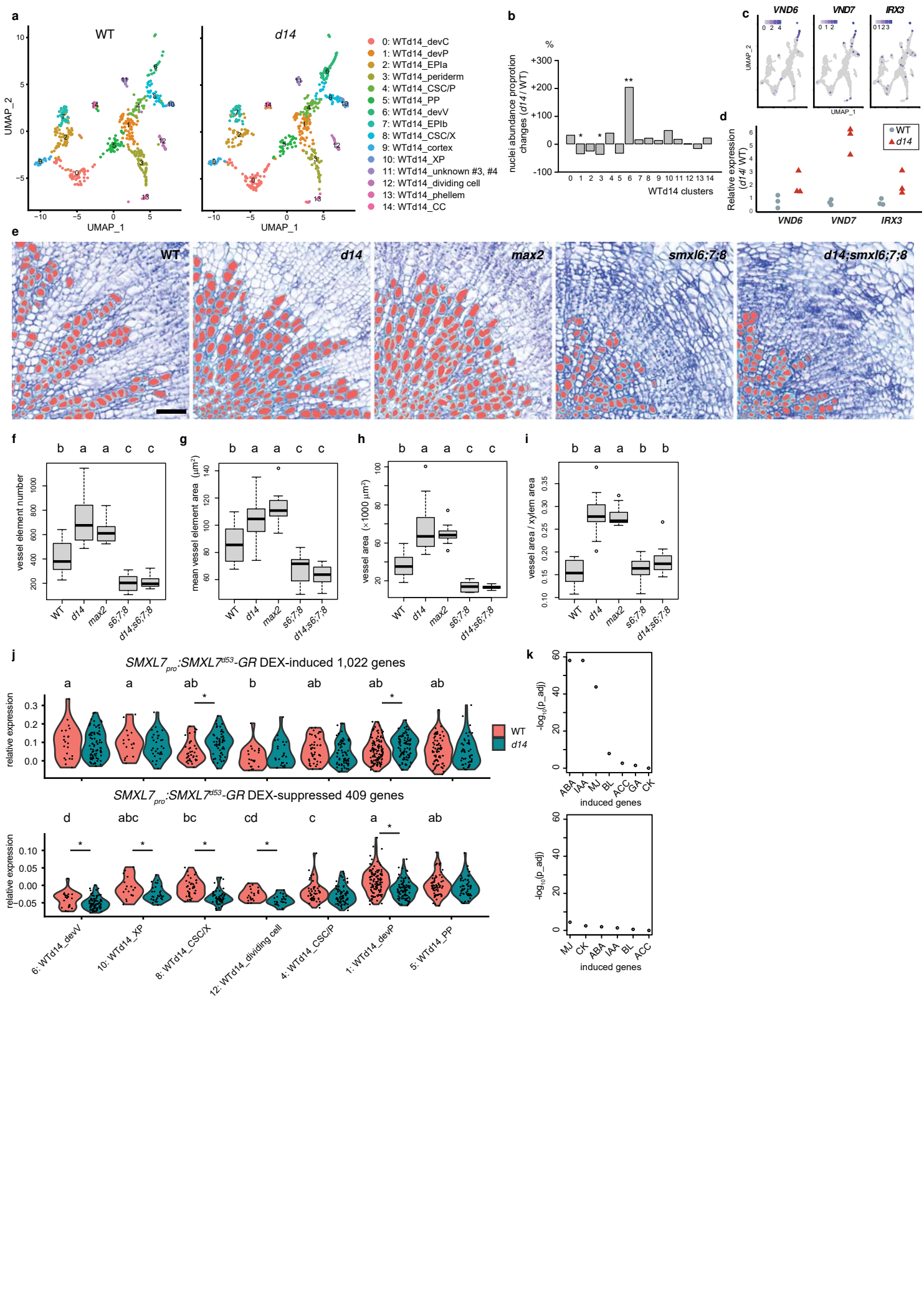
a
WT
d14
UMAP_2
UMAP_1
0: WTd14_devC
1: WTd14_devP
2: WTd14_EPIa
3: WTd14_periderm
4: WTd14_CSC/P
5: WTd14_PP
6: WTd14_devV
7: WTd14_EPIb
8: WTd14_CSC/X
9: WTd14_cortex
10: WTd14_XP
11: WTd14_unknown #3, #4
12: WTd14_dividing cell
13: WTd14_phellem
14: WTd14_CC
b
nuclei abundance proprotion changes (d14 / WT)
%
WTd14 clusters
c
VND6
VND7
IRX3
d
Relative expression (d14/ WT)
WT
d14
e
WT
d14
max2
smxl6;7;8
d14;smxl6;7;8
f
vessel element number
g
mean vessel element area (μm²)
h
vessel area (×1000 μm²)
i
vessel area / xylem area
WT
d14
max2
s6;7;8
d14;s6;7;8
j
SMXL7pro:SMXL7d53-GR DEX-induced 1,022 genes
SMXL7pro:SMXL7d53-GR DEX-suppressed 409 genes
relative expression
WT
d14
6: WTd14_devV
10: WTd14_XP
8: WTd14_CSC/X
12: WTd14_dividing cell
4: WTd14_CSC/P
1: WTd14_devP
5: WTd14_PP
k
-log10(p_adj)
induced genes
ABA
IAA
MJ
BL
ACC
GA
CK

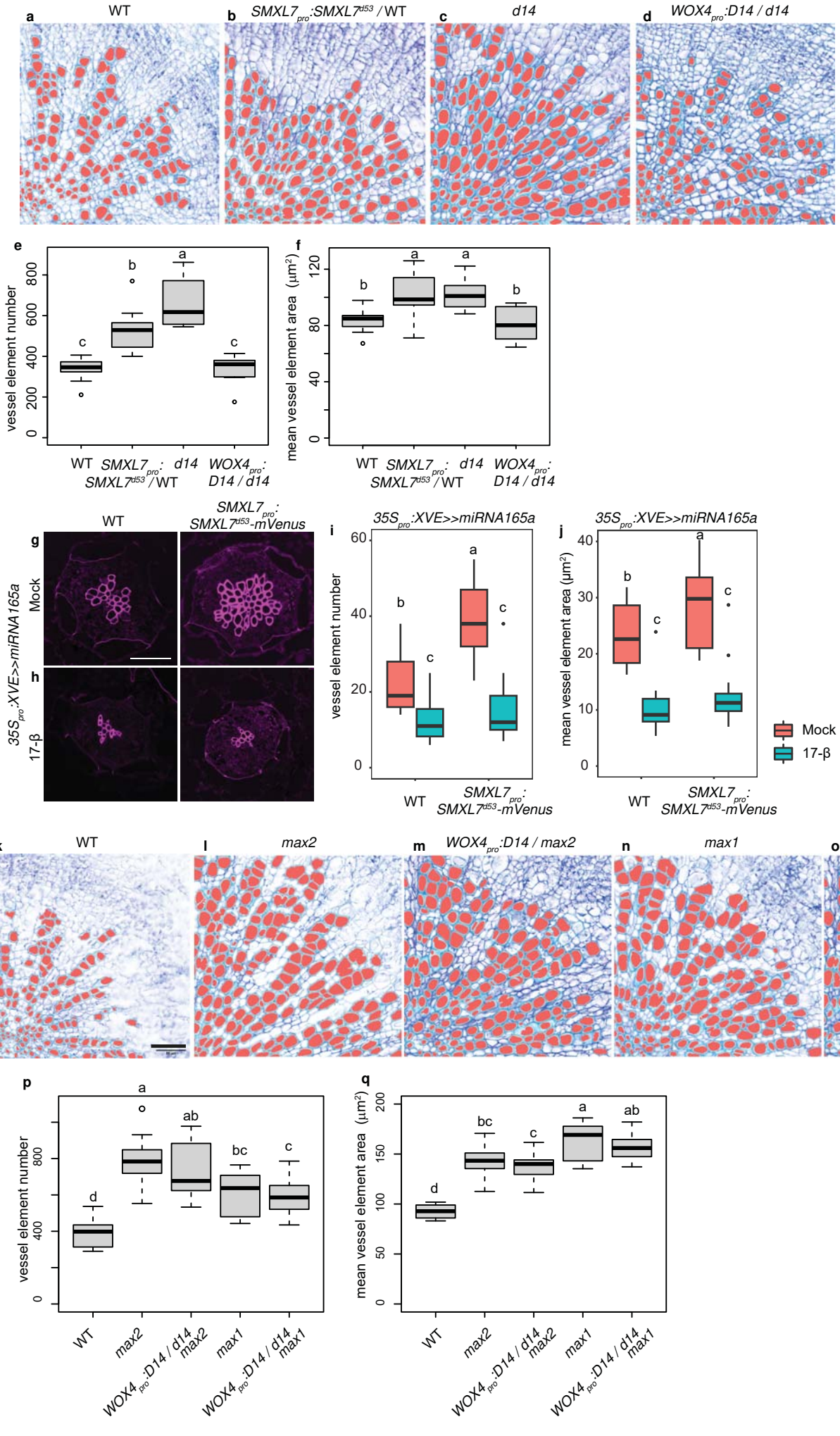
a
WT
b
SMXL7pro:SMXL7d53 / WT
c
d14
d
WOX4pro:D14 / d14
e
vessel element number
0
200
400
600
800
WT
SMXL7pro: SMXL7d53 / WT
d14
WOX4pro: D14 / d14
f
mean vessel element area (µm2)
0
40
80
120
g
WT
SMXL7pro: SMXL7d53-mVenus
35Spro:XVE>>miRNA165a
Mock
h
17-β
i
35Spro:XVE>>miRNA165a
vessel element number
0
20
40
60
WT
SMXL7pro: SMXL7d53-mVenus
j
35Spro:XVE>>miRNA165a
mean vessel element area (µm2)
0
10
20
30
40
Mock
17-β
k
WT
l
max2
m
WOX4pro:D14 / max2
n
max1
o
WOX4pro:D14 / max1
p
vessel element number
0
400
800
WT
max2
WOX4pro:D14 / d14 max2
max1
WOX4pro:D14 / d14 max1
q
mean vessel element area (µm2)
0
50
100
150
200
WT
max2
WOX4pro:D14 / d14 max2
max1
WOX4pro:D14 / d14 max1

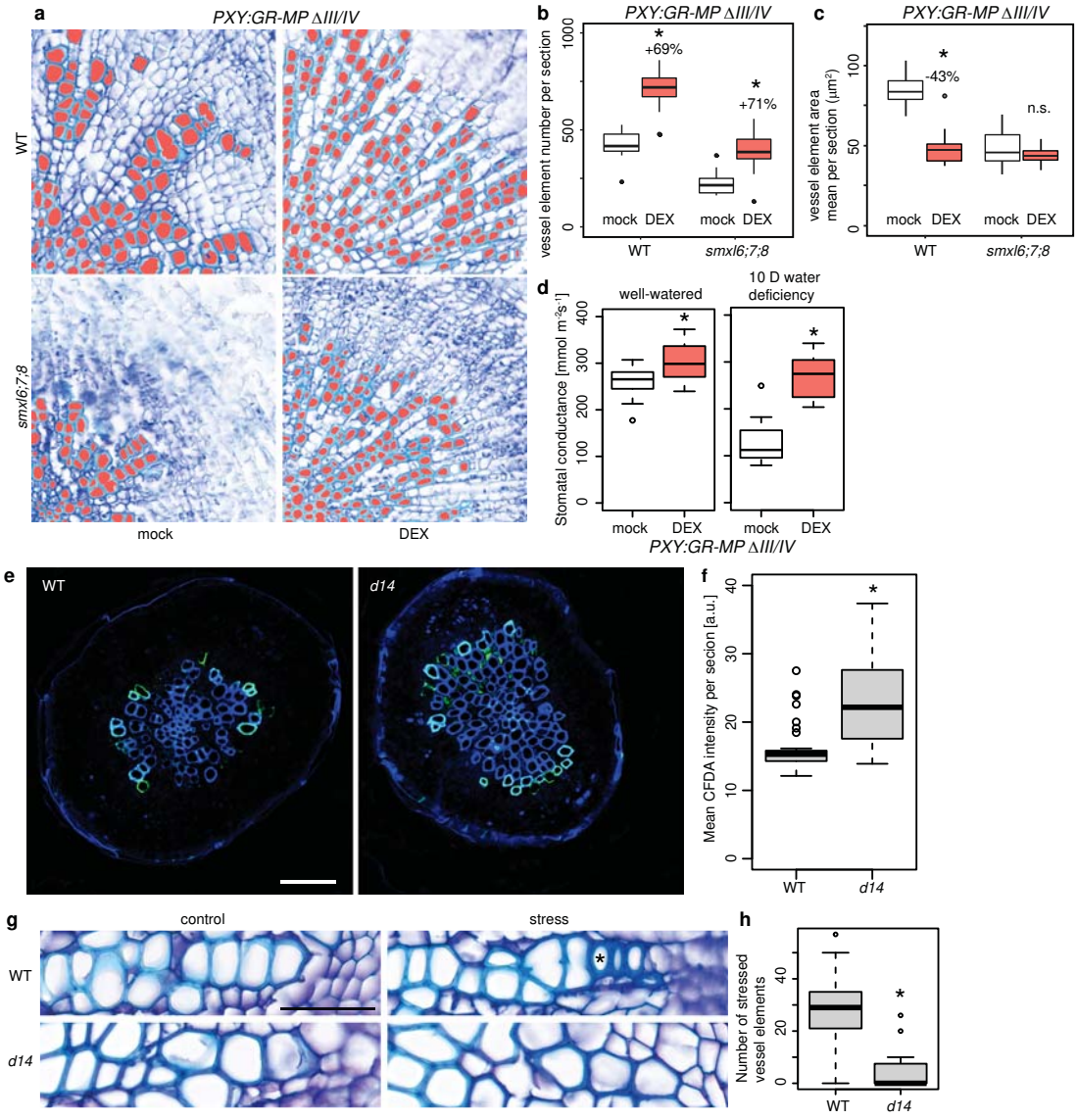
a
PXY:GR-MP ΔIII/IV
WT
smxl6;7;8
mock
DEX
b
PXY:GR-MP ΔIII/IV
vessel element number per section
+69%
+71%
mock DEX mock DEX
WT
smxl6;7;8
c
PXY:GR-MP ΔIII/IV
vessel element area mean per section (μm²)
-43%
n.s.
mock DEX mock DEX
WT
smxl6;7;8
d
well-watered
10 D water deficiency
Stomatal conductance [mmol m⁻²s⁻¹]
mock DEX mock DEX
PXY:GR-MP ΔIII/IV
e
WT
d14
f
Mean CFDA intensity per secion [a.u.]
WT
d14
g
control
stress
WT
d14
h
Number of stressed vessel elements
WT
d14